Geophysical Journal International

Geophys. J. Int. (2011) **186,** 385–389 doi: 10.1111/j.1365-246X.2011.05089.x

EXPRESS LETTER

Crustal thickness and *Vp*/*Vs* ratio of the central and western North China Craton and its tectonic implications

Zigen Wei, Ling Chen and Weiwei Xu

State Key Laboratory of Lithospheric Evolution, Institute of Geology and Geophysics, Chinese Academy of Sciences, Beijing 100029, China. E-mail: weizigen@mail.iggcas.ac.cn

Accepted 2011 May 24. Received 2011 March 10; in original form 2010 September 18

SUMMARY

We obtained the crustal thickness (H) and average Vp/Vs ratio (κ) for the central (CNCC) and western North China Craton (WNCC) by H–κ stacking of receiver functions. Our results show that H and κ varies significantly but similarly in the northern and southern CNCC, reflecting possible effects of the Phanerozoic cratonotic reactivation on the region. Of the WNCC, the south is featured by κ values typical for Precambrian shields ($\sim$1.77) and variations of H mirroring surface topography; the north presents large fluctuations of κ (1.68–1.93) and a crustal thickening (up to 50 km) uncorrelated with topography. Such N–S differences were thought to be associated with a $\sim$1.95-Ga suturing event occurred in the north with little effects on the south. Our observations suggest that distinct structural heterogeneities of the NCC not only reflect diverse regional tectonics in Phanerozoic, but also provide evidence for long-term survival of crustal fabrics in stable continental interior.

Key words: Body waves; Cratons; Crustal structure; Asia.

1 INTRODUCTION

The North China Craton (NCC, Fig. 1), consisting of the eastern and western NCC of Archean age and the Paleoproterozoic Trans-North China Orogen (central NCC) between them, is one of the oldest cratons in the world (Liu *et al.* 1992). Unlike typical cratons that are underlain by a thick and strong lithosphere and have been tectonically stable for billions of years, the eastern NCC underwent significant thermotectonic reactivation and destruction in the Phanerozoic, with both the lithospheric mantle (e.g. Menzies *et al*. 1993; Griffin *et al*. 1998; Chen *et al*. 2008) and the crust (e.g. Gao *et al*. 1998; Zheng *et al*. 2006) having been severely modified and thinned. The Phanerozoic evolution of the central and western NCC is still debated, given the coexistence of both substantially thinned and preserved thick lithosphere (Chen *et al*. 2009), marked structural (e.g. Zheng *et al*. 2009; Zhao *et al*. 2009) and chemical heterogeneities (e.g. Xu 2007; Tang *et al*. 2008) in the crust and lithospheric mantle. Recent high-resolution seismic images (e.g. Chen *et al*. 2009; Zhao *et al*. 2009) as well as geochemical and petrological data (e.g. Xu 2007; Tang *et al*. 2008) suggest that lithospheric remobilization and thinning probably also took place in this region, but mainly confined to the elongated Cenozoic rift systems (Yinchuan-Hetao and Shaanxi-Shanxi rifts, Fig. 1); These rift systems surround the stable Ordos Block in the western NCC where a thick lithosphere of $\sim$200 km remains preserved (Chen *et al*. 2009; Zhao *et al*. 2009). This together with the rapid changes in topography and gravity field (as marked by the North–South Gravity Lineament, or NSGL) near the boundary between the eastern and central NCC (Fig. 1) indicate that the central and western NCC may have evolved tectonically differently from their eastern counterpart (Xu 2007; Chen 2010).

To better understand the heterogeneous structure of the central and western NCC and associated tectonic processes, in this study we investigate the lateral variations in the crustal thickness and ratio of *P* and *S* wave speeds using the teleseismic receiver function (RF) data recorded at dense seismic arrays. We mainly focus on the different structural features between the northern and southern parts of the Ordos Block.

2 DATA AND METHOD

Teleseismic data used in this study come from 128 temporary seismic stations along two profiles traversing the northern and southern parts of the central and western NCC, respectively. These stations belong to three seismic arrays (II, IV and V) of the Northern China Interior Structure Project (NCISP). More details of the NCISP experiments can be found in Zhao *et al*. (2009) and references therein. We selected three-component waveform data from earthquake events with magnitude $\geq$5.5 and epicentral distance ranging from 28° to 90° and calculated the RFs using a time-domain

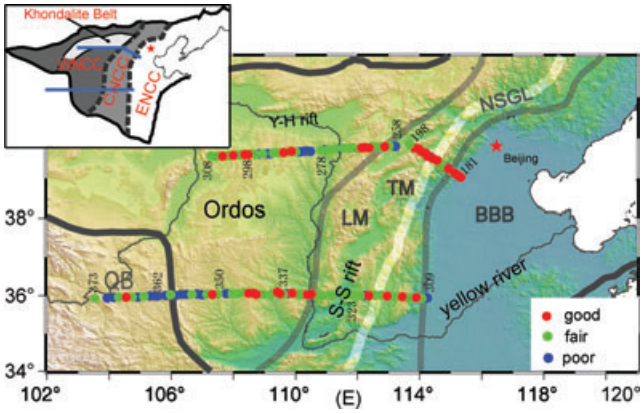

Figure 1. Map showing the study region and seismic stations (circles). Black lines denote the boundary of the North China Craton (NCC) and two grey lines outline the central NCC (Zhao *et al*. 2005). Circles with different colours indicate different data qualities of the stations. Thick white line marks the North–South Gravity Lineament (NSGL). WNCC, CNCC and ENCC denote the western, central and eastern NCC, respectively. BBB: Bohai Bay Basin; TM: Taihang Mountains; LM: Lüliang Mountains; Y-H rift: Yinchuan-Hetao rift; S-S rift: Shaanxi-Shanxi rift; Ordos: Ordos Plateau; QB: Qilian Block. Map inset shows the threefold subdivision of the NCC (Zhao *et al*. 2005). The two blue lines represent the seismic arrays used in this study.

maximum entropy deconvolution method, similarly as described in the previous studies (e.g. Xu & Zheng 2005). After removing bad traces that look obviously different from the majority, we ended up with ∼19 000 high-quality RFs (Table S1) for further analysis. The back azimuths of this data set mainly concentrate between 100° and 220° (Fig. S1).

We used the RF H–κ stacking method (Zhu & Kanamori 2000) to determine the average crustal thickness (H) and the ratio of P- and S-wave velocities (Vp/Vs ratio, or κ) under each station. This method treats the crust as a single homogeneous layer, and constrains H and κ of the crust by searching the most energetic stack of the direct Ps phase and multiples such as $PpPs$, $PsPs$+$PpSs$ of the Moho according to the predicted delays relative to the incident P wave. In this regard, identification of the relevant phases in the RFs (the data quality) is important to achieve reliable H–κ stacking results. We therefore ranked the stations into three categories (Fig. 1): 'good' (36 stations), 'fair' (64 stations) and 'poor' (28 stations), according to the quality of the RFs (see auxiliary materials for examples).

In addition to the data quality, we also considered a number of key parameters which may affect the estimates of H and κ. The first one is the frequency range. We tested various sets of cut-off frequencies and investigated the frequency dependency of the H and κ estimates for each station. We found that for our data set the range of 0.03–0.5 Hz is the best to balance the trade-off between suppression of high-frequency noise and resolution preservation. The frequency dependency of the results will be described and discussed in the next section. The second one is the average crustal P wave velocity ($\overline{Vp}$). In our case, H generally increases by 0.6–0.8 km with a 0.1 km s^{-1} increase in $\overline{Vp}$. κ is less sensitive to $\overline{Vp}$. Changing $\overline{Vp}$ from 6.0 to 7.0 km s^{-1} in the H–κ stacking, the resultant κ varies by no more than 0.05 for all the stations. Reasonable values of $\overline{Vp}$ are 6.4, 6.3 and 6.25 km s^{-1} for the entire northern profile, the Qilian Block and southern Ordos, and the southern part of the central NCC, respectively, as suggested by previous studies using both seismic exploration (e.g. Jia *et al*. 1995) and earthquake data (Zheng *et al*. 2006, 2009). We therefore adopted these $\overline{Vp}$ values to derive the best estimates of H and κ along the two profiles. Finally, we chose unequal weights (0.6, 0.3 and 0.1) for Ps, $PpPs$ and $PpSs$+$PsPs$ phases of the Moho, respectively, in H–κ stacking of RFs. Using other sets of weights did not lead to noticeable changes of the results.

It is worth mentioning that sometimes the output of H–κ stacking was nonunique. In this case, we determined the H and κ values by referring to previous studies and comparing with neighbouring stations. To quantitatively estimate the uncertainty of our results, we measured the error bars for H and κ by taking into account the uncertainties of all the parameters mentioned above and integrating the 95% confidence intervals for individual parameters.

3 RESULTS

Fig. 2 shows the estimated crustal thickness, Vp/Vs ratio with error bars and representative velocity models for the northern and southern profiles, respectively. For comparison, the topography is also plotted with main tectonic units and boundaries labelled on the top of the figure. In the eastern portion of both profiles, the crust thickens from ∼30 km near the boundary between the eastern and central NCC to >40 km when entering the western NCC, with an apparent thinning beneath the Cenozoic Shaanxi-Shanxi rift areas in the central NCC (Figs 2b and e). Such variations in crustal thickness approximately mirror the surface topography of the region (Figs 2a and d). The Vp/Vs ratios in this portion of the two profiles also vary similarly, with relatively higher values appearing under the rift areas and around the boundary between the eastern and central NCC (Figs 2c and f). Our results for the northern part of the central NCC agree well with the previous study by Xu & Zheng (2005) who studied the crustal structure of this area using the same method.

Unlike the similar structural feature in the central NCC, striking differences are obvious in both the crustal thickness and Vp/Vs ratio between the two profiles within the western NCC. First, the crustal thickness along the southern profile monotonously increases westward till reaching the western border of the Ordos Block, and continuously mirrors the topography even under the Qilian Block further to the west (Fig. 2e). In contrast, the crust along the northern profile is relatively thin at both edges and appears the thickest in the interior of the Ordos Block, inconsistent with the topography (Fig. 2b). It is worth noting that such variation patterns of the crustal thickness obtained from RF H–κ stacking for both profiles agree with those derived from waveform inversion of RFs (Zheng *et al*. 2009; Zhu & Zheng 2009), although the absolute thicknesses for the northern profiles differ to some extent (up to 6 km) (Fig. 2b). Second, the Vp/Vs ratio varies substantially along the northern profile, showing a distinct change from low values around 1.73 to high ones >1.82 near the thickest crust area and then a decrease to ∼1.78 in the western Ordos (Fig. 2c). On the other hand, the Vp/Vs ratio along the southern profile only exhibits subtle fluctuations around the average value of 1.77 within the Ordos Block (Fig. 2f), comparable to that of typical Precambrian shield (Zandt *et al*. 1995).

It is interesting to note that the crustal thicknesses in the northern Ordos obtained in this study from RF H–κ stacking are always larger than those derived by Zheng *et al*. (2009) based on waveform inversion of RFs (Fig. 2b). To understand this discrepancy, we investigated the velocity model for each station from Zheng *et al*. in detail. We found that under most stations where there is a large difference between the two results, the S velocity either increases gradually with depth or changes rapidly at two or more

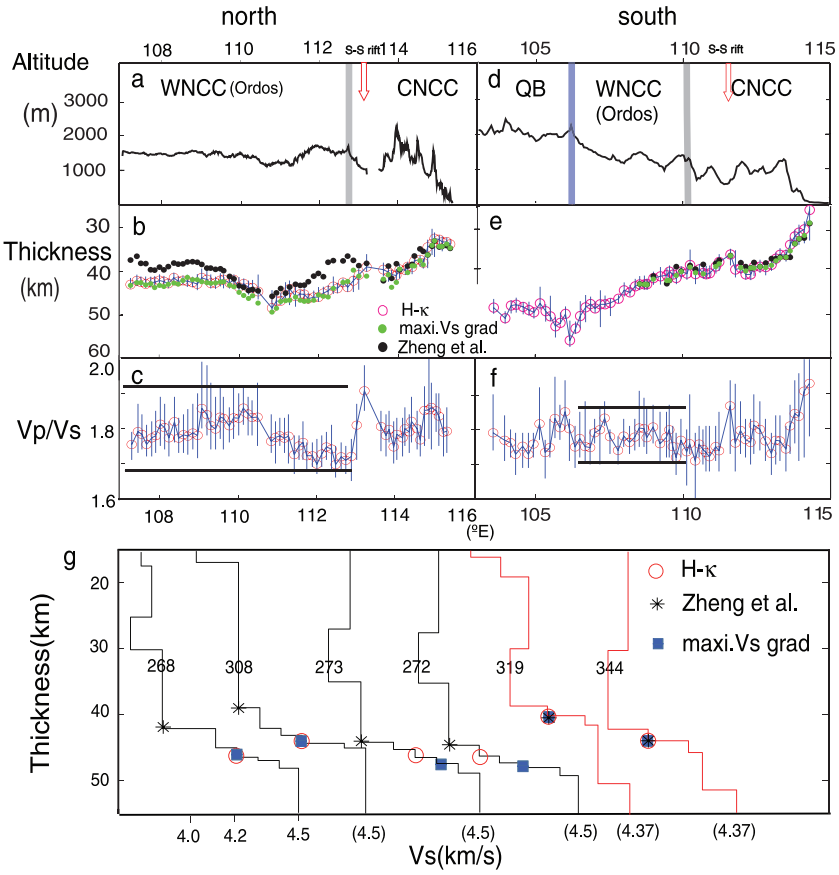

Figure 2. Comparison of altitude (a, d), crustal thickness (H) (b, e), Vp/Vs ratio (κ) (c, f) and crustal velocity structure (g) between the northern and southern profiles. Red arrows in (a, d) mark the location of Shaanxi-Shanxi rift (S-S rift). Red circles and blue bars in (b, c, e, f) represent the best estimates of H and κ and errors by taking into account the uncertainties of key parameters used in the H–κ stacking of RFs. Black filled circles in (b, e) give the Moho depths derived from waveform inversion of RFs (Zheng *et al*. 2009; Zhu & Zheng 2009), and green ones denote the depths of maximum velocity gradient in the range of 4.0–4.5 km s^{-1}. Black lines in (c, f) manifest the variation range of κ in the western NCC. In (g), velocity models (Zheng *et al*. 2009; Zhu & Zheng 2009) for representative stations of the northern and southern profiles are plotted in black and red, respectively, with the Moho depths estimated using different methods marked.

depths around the base of the crust (e.g. black lines in Fig. 2g). We also measured the velocity gradients based on Zheng *et al*.'s models and took the depth at which the S velocity gradient is the highest within the velocity range of 4.0–4.5 km s^{-1} as the Moho depth. The so-obtained crustal thicknesses under most stations are consistent with the H–κ stacking results, but again larger than those from Zheng *et al*. (2009) for the northern Ordos (Figs 2b, e and g).

Besides the different dependences of the crustal thickness estimates on the adopted method, we also found that the values of crustal thicknesses obtained from RF H–κ stacking vary distinctly differently with frequency between the southern and northern Ordos. The crust thickness mapped for the southern Ordos is not sensitive to the frequencies used (variations <1 km for almost all the stations). However, for the northern Ordos, smaller values of crust thickness were obtained when using lower frequencies data. In particular, changing the frequency range from 0.03–0.5 Hz to 0.03–0.3 Hz resulted in a decrease of crust thickness by 2–4 km for most stations. The agreement and discrepancies in the crustal thickness using various methods and different frequency contents of data may reflect different structural features of the crust–mantle transition (CMT) in the northern and southern parts of the Ordos region. The CMT is probably sharp in the southern Ordos, such that the Moho was well defined and its depths were consistently estimated based on either technique (Figs 2e and g). On the other hand, a relatively thick CMT zone may exist under the northern Ordos. The Moho proposed by Zheng *et al*. (2009) (above which the S velocities are no larger than 3.9 km s^{-1}) is almost exclusively located around the top of the CMT (black symbols in Fig. 2g). Those estimated from H–κ stacking of RFs appears either close to the depth of maximum velocity gradient or near the middle of the CMT (red circles in Fig. 2g) and are more sensitive to the frequencies used, consistent with recent synthetic modelling results for a thick lowermost crustal layer structure (Rumpfhuber *et al*. 2009).

4 DISCUSSION

To further gain insight into the nature of the crust and tectonic evolution in the central and western NCC, we compared the crustal thicknesses with the Vp/Vs ratios and altitudes measured at all the 128 stations and studied their variations with regional geology (Fig. 3).

We found that in the central NCC the Vp/Vs ratio increases nearly linearly as the crustal thickness decreases, though with slightly different changing rates between the north and south (Fig. 3a). Such a linear H–κ relation could be attributed to a balance between the

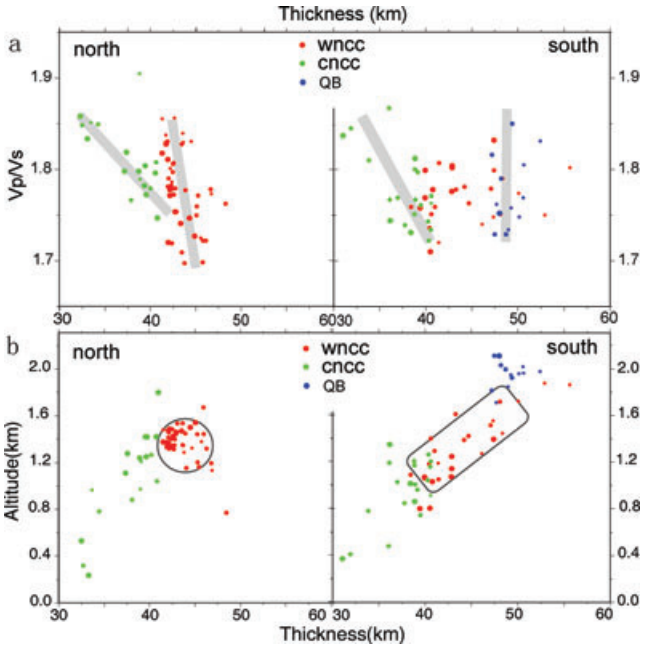

Figure 3. *Vp*/*Vs* ratio versus crustal thickness (a) and altitude versus crustal thickness (b) for all the 128 stations considered in this study. Large, medium and small dots represent the *H*–κ stacking results from RFs falling in the 'good', 'fair' and 'poor' categories, respectively. Different colours stand for different regions. In (a), the grey bars give the approximate variation trends for individual regions. In (b), the circle and the rectangle show the different variation trends in the northern and southern Ordos.

opposing contributions of tectonic thinning of felsic upper-crust (a increase in κ with decreasing H) and addition of mafic materials through basaltic underplating (a increase in κ with increasing H; Ji *et al*. 2009); both processes were reported to have taken place in the central NCC since Mesozoic (e.g. Chen *et al*. 2001; Zhang *et al*. 2003). These together with the similar variation patterns of the crustal structure in the northern and southern parts of the central NCC (Fig. 2) suggests that the Phanerozoic tectonothermal reactivation processes may have affected these areas in a same manner (but probably to somewhat different extents). In addition, the localized thinning and distinctly high *Vp*/*Vs* ratios of >1.85 right beneath the Shaanxi-shanxi rift areas (Fig. 2) corroborate previous geochemical and geophysical observations that cratonic reactivation in the central NCC is particularly pronounced in the Cenozoic rift systems (e.g. Xu 2007; Tang *et al*. 2008; Chen *et al*. 2009).

In the western NCC, the *H*–κ relation not only appears different from that in the central NCC, but also differs significantly between the northern and southern Ordos (Fig. 3a), similar as but more distinct than individual parameters (Fig. 2). The southern Ordos shows no clear correlation between H and κ with relatively smaller fluctuations of κ, whereas the northern Ordos displays a *H*–κ variation trend intermediate between that in the central NCC to the east and in the Qilian Block to the west (Fig. 3a). The Qilian Block is featured by a nearly constant crustal thickness but obviously varying *Vp*/*Vs* ratios, reflecting strong lateral heterogeneity in the crust, probably associated with the Paleozoic or Cenozoic active tectonics of the region.

The variations in the crustal thickness versus surface topography are also much different between the northern and southern Ordos. As shown in Fig. 3(b), while the crust thickness increases with the altitude in the south, roughly along the same trend in the central NCC and the Qilian Block, no clear variation trend is observed in the north. Assuming isostatic compensation in the crust which is reasonable for the stable regions in the western NCC, the correspondence between an increase of crustal thickness and a depression of topography in the middle part of the Northern Ordos (Figs 2a and b) would indicate a relatively denser crust at this area compared with surrounding regions.

The large differences in both the relations of crustal thickness versus *Vp*/*Vs* ratio and crustal thickness versus surface topography (Fig. 3) and the CMT sharpness (Figs 2b, e and g) strongly suggest significant variations in the crustal structure within the Ordos Block in the western NCC. The sharp Moho and the stable *Vp*/*Vs* ratios around 1.77 in the southern Ordos are typical features of the Archean cratons in the world (Griffin *et al*. 1987; Niu *et al*. 2002). This, combined with the low heat flow, little seismicity and magmatic activity, no internal deformation since the Precambrian (e.g. Zhai & Liu 2003), and the presence of a thick and high-velocity mantle root (Zhao *et al*. 2009), suggests that the crust as well as the lithospheric mantle under the southern Ordos may have not been disturbed noticeably since Archean and have retained its cratonic nature and stability over long periods of geological time.

Compared with the southern Ordos, the obvious fluctuations of both the crustal thickness and *Vp*/*Vs* ratio and the structural feature of the CMT in the northern Ordos may indicate the occurrence of tectonic modification that was absent or had minor effects on the southern Ordos. RF waveform inversion results from Zheng *et al*. (2009) and Zhu & Zheng (2009) revealed a large-scale low velocity zone dipping from the shallow crust to the lower crust under both the northern and southern Ordos Block, which the authors interpreted as a remnant of upper-middle continental crust subducted during the final assembly of the eastern and western NCC at $\sim$1.85 Ga (Zhao *et al*. 2005). This interpretation therefore implies that the crust of both areas was affected similarly by the Paleoproterozoic cratonic assembly process and has not been disturbed noticeably since then. If it is correct, then the crustal modification in the northern Ordos inferred here could not be attributed to the $\sim$1.85 Ga event, but more likely happened earlier than it. Given the proximity of the northern profile to the Khondalite Belt (inset in Fig. 1) along which the Ordos Block and the Yinshan Block collided and amalgamated to form the western NCC at $\sim$1.95 Ga (Zhao *et al*. 2005), we speculate that this ancient continental collision event may have contributed to the crustal modification in the northern Ordos. The collision process and associated magmatism may have affected the crustal structure of the Khondalite Belt and adjacent areas through heterogeneous mafic intrusion and/or possible magmatic underplating, resulting in locally thickened crust, increased *Vp*/*Vs* ratios and a thick and denser CMT zone in the region (Fig. 2). Indeed, the crustal structure in the northern Ordos resembles that of many other cratonic regions where early Proterozoic tectonics appears to be dominant in shaping the deep structure (e.g. BABEL Working Group 1990; White *et al*. 2000; Crosswhite & Humphreys 2003). Our observations therefore provide an excellent example of significant structural variations in a craton interior, and lend further support for the long-term (thousands of million years) survival of crustal fabrics developed in the early evolution of stable continents.

5 CONCLUSIONS

Our results from *H*–κ stacking of dense array RFs reveal complex crustal structures of the NCC, reflecting possible Phanerozoic tectonothermal reactivation of the central NCC but long-term stability of the western NCC. Our observations together with the widely reported distinct structure and fundamental destruction of

the eastern NCC suggest that the present-day significant structural heterogeneities of the craton are associated with complex and diverse geology and tectonics of the region, probably not only in the Phanerozoic evolution but also during ancient eras before its cratonization.

ACKNOWLEDGMENTS

We are thankful to the Seismic Array Laboratory in the Institute of Geology and Geophysics, Chinese Academy of Sciences for providing the data. We thank Tianyu Zheng, Liang Zhao and Mingming Li for beneficial discussions. This research is supported by the National Science Foundation of China (Grants 90814002 and 90914011). Ling Chen gratefully acknowledges the support of K.C.Wong Education Foundation, Hong Kong.

REFERENCES

BABEL Working Group., 1990. Evidence for early Proterozoic plate tectonics from seismic reflection profiles in the Baltic shield, *Nature,* **348,** 34–38.

Chen, L. *et al.*, 2008. Distinct lateral variation of lithospheric thickness in the northeastern North China Craton, *Earth planet. Sci. Lett.,* **267,** 56–68.

Chen, L., Cheng, C. & Wei, Z., 2009. Seismic evidence for significant lateral variations in lithospheric thickness beneath the central and western North China Craton, *Earth planet. Sci. Lett.,* **286,** 171–183.

Chen, L., 2010. Concordant structural variations from the surface to the base of the upper mantle in the North China Craton and its tectonic implications, *Lithos,* **120,** 96–115, doi:10.1016/j.lithos.2009.12.007.

Chen, S. *et al.*, 2001. Thermal and petrological structure of the lithosphere beneath Hannuoba, Sino-Korean Craton, China: evidence from xenoliths, *Lithos,* **56,** 267–301.

Crosswhite, J. A. & Humphreys, E. D., 2003. Imaging the mountainless root of the 1.8 Ga Cheyenne belt suture and clues to its tectonic stability, *Geology,* **31,** 669–672.

Gao, S. *et al.*, 1998. Chemical composition of the continental crust as revealed by studies in East China, *Geochim. Cosmochim. Acta.,* **62,** 1959–1975.

Griffin, W. L, & O'Reilly, S.Y., 1987. The composition of the lower crust and the nature of the continental Moho-xenolith evidence, in *Mantle Xenoliths,* pp. 413–432, ed. Nixon, P.H., John Wiley and Sons, Chichester.

Griffin, W. L. *et al.*, 1998. Phanerozoic evolution of the lithosphere beneath the Sino-Korean craton, in *Mantle Dynamics and Plate Interactions in East Asia,* Geodyn. Ser. Vol. 27, pp. 107– 126, eds Flower, M. F. J., *et al*., AGU, Washington, DC.

Ji, S., Wang, Q. & Salisbury, M. H., 2009. Composition and tectonic evolution of the Chinese continental crust constrained by Poisson's ratio, *Tectonophysics,* **463,** 15–30.

Jia, S. & Liu, C., 1995. Study on the seismic phase of DSS in North China, *Seismol. Geol.,* **17**(2), 97–105.

Liu, D. *et al.*, 1992. Remnants of 3800 Ma crust in the Chinese part of the Sino-Korean craton, *Geology,* **20,** 339–342.

Menzies, M. A., Fan, W. M. & Zhang, M., 1993. Palaeozoic and Cenozoic lithoprobes and the loss of N120 km of Archaean lithosphere, Sino-Korean Craton, China, *Geol. Soc. London Spec. Pub.,* **76,** 71–78.

Niu, F. & James, D. E., 2002. Fine structure of the lowermost crust beneath the Kaapvaal craton and its implications for crustal formation and evolution, *Earth planet. Sci. Lett.,* **200,** 121–130.

Rumpfhuber, E. –M. *et al.*, 2009. Rocky Mountain evolution: tying continental dynamics of the Rocky Mountains and deep probe seismic experiments with receiver functions, *J. geophys. Res.,* **114,** B08301, doi:10.1029/2008JB005726.

Tang, Y. *et al.*, 2008. Refertilization of ancient lithospheric mantle beneath the central North China Craton: evidence from petrology & geochemistry of peridotite xenoliths, *Lithos,* **101,** 435–452.

White, D. J., Zwanzig, H. V. & Hajnal, Z., 2000. Crustal suture preserved in the paleoproterozoic Trans-Hudson orogen, Canada, *Geology,* **28,** 527–530.

Xu, W. & Zheng, T., 2005. Distribution of Poisson's ratios in the northwestern basin—mountain boundary of the Bohai Bay Basin, *Chin. J. Geophys.,* **48**(5), 1077–1084.

Xu, Y., 2007. Diachronous lithospheric thinning of the North China Craton and formation of the Daxin'anling—Taihangshan gravity lineament, *Lithos.,* **96,** 281–298.

Zandt, G. & Ammon, C. J., 1995. Continental crust compostion constrained by measurements of crustal Poisson's ratio, *Nature,* **374,** 152–154.

Zhai, M. & Liu, W., 2003. Paleoproterozoic tectonic history of the North China craton: a review, *Precambrian Res.,* **122**: 183–199.

Zhang, Y. Q. *et al.*, 2003. Cenozoic extensional stress evolution in North China, *J. Geodyn.,* **36,** 591–613.

Zhao, G. *et al.*, 2005. Late Archean to Paleoproterozoic evolution of the North China Craton: key issues revisited, *Precambrian Res.,* **136,** 177–202.

Zhao, L. *et al.*, 2009. Reactivation of an Archean craton: constraints from P- & S-wave tomography in North China, *Geophys. Res. Lett.,* **36,** L17306, doi:10.1029/2009GL039781.

Zheng, T. *et al.*, 2006. Crust–mantle structure difference across the gravity gradient zone in North China Craton: seismic image of the thinned continental crust, *Phys. Earth planet. Inter.,* **159,** 43–58.

Zheng, T., Zhao, L., & Zhu, R., 2009. New evidence from seismic imaging for subduction during assembly of the North China Craton, *Geology,* **37**(5), 395–398.

Zhu, L. & Kanamori, H., 2000. Moho depth variation in southern California from teleseismic receiver functions, *J. geophys. Res.,* **105**, 2969–2980.

Zhu, R. & Zheng, T., 2009. Destruction geodynamics of the North China Craton and its Paleoproterozoic plate tectonics. *Chin. Sci. Bull.,* **54,** doi:10.1007/s11434–009-0451–5.

SUPPORTING INFORMATION

Additional Supporting Information may be found in the online version of this article:

Supplement. This material contains information of the RF data set (Table S1 and Fig. S1) and the corresponding H–κ results for representative stations of different categories (Fig. S2).

Please note: Wiley-Blackwell are not responsible for the content or functionality of any supporting materials supplied by the authors. Any queries (other than missing material) should be directed to the corresponding author for the article.